BRIEF REPORT

Pseudobudding: ruptured glands do not represent true tumor buds

Tariq Sami Haddad[1]*[iD], Luuk van den Dobbelsteen[1], Sonay K Öztürk[1], Robin Geene[2], Isaäc J Nijman[2], Kiek Verrijp[1], Nigel B Jamieson[3], Colin Wood[3][iD], Shannon van Vliet[1], Luuk Reuvers[1], Soumia Achouiti[1], Natasja Rutgers[1], Nelleke Brouwer[1], Femke Simmer[1], Inti Zlobec[4], Alessandro Lugli[4] and Iris D Nagtegaal[1]

[1] Radboud University Medical Center, Nijmegen, The Netherlands
[2] USEQ, CMM, University Medical Center Utrecht, Utrecht, The Netherlands
[3] University of Glasgow, Wolfson Wohl Cancer Research Centre, School of Cancer Sciences, Glasgow, UK
[4] Institute of Tissue Medicine and Pathology, University of Bern, Bern, Switzerland

*Correspondence to: TS Haddad, Department of Pathology, RadboudUMC, 6525 GA Nijmegen, The Netherlands.
E-mail: tariq.haddad@radboudumc.nl

Abstract

Tumor budding (TB) is a strong biomarker of poor prognosis in colorectal cancer and other solid cancers. TB is defined as isolated single cancer cells or clusters of up to four cancer cells at the invasive tumor front. In areas with a large inflammatory response at the invasive front, single cells and cell clusters surrounding fragmented glands are observed appearing like TB. Occurrence of these small groups is referred to as pseudobudding (PsB), which arises due to external influences such as inflammation and glandular disruption. Using a combination of orthogonal approaches, we show that there are clear biological differences between TB and PsB. TB is representative of active invasion by presenting features of epithelial–mesenchymal transition and exhibiting increased deposition of extracellular matrix within the surrounding tumor microenvironment (TME), whereas PsB represents a reactive response to heavy inflammation where increased levels of granulocytes within the surrounding TME are observed. Our study provides evidence that areas with a strong inflammatory reaction should be avoided in the routine diagnostic assessment of TB.

© 2023 The Authors. *The Journal of Pathology* published by John Wiley & Sons Ltd on behalf of The Pathological Society of Great Britain and Ireland.

Introduction

Tumor budding (TB) is defined as isolated single cancer cells or clusters up to four cancer cells located at the invasive margin of colorectal cancer (CRC) [1]. TB is firmly established as a strong and independent predictor of lymph node metastasis, disease recurrence, and cancer-related deaths [2]. Pseudobudding (PsB), in contrast to TB, is defined as isolated single cancer cells or clusters of up to four cells at the invasive front that occur due to gland disruption and external influences such as inflammation [3]. PsB may be confused with true TB, yet their biology likely differs. No studies to date have investigated the molecular backgrounds of these two features and whether they are truly biologically distinct. Here we investigate TB and PsB using spatial transcriptomic, multiplex immunofluorescent, immunohistochemical, three-dimensional (3D), and super-resolution-based approaches to gain insight into their underlying biology.

Materials and methods

Cases and tissue material

This study included resection material from 21 CRC cases at the Radboud University Medical Center (RadboudUMC), where TB and PsB regions were observed (supplementary material, Table S1). Pathologists (SKO, IDN) were guided and selected TB and PsB regions based on a review of cases according to the International Tumor Budding Consensus Conference (ITBCC) 2016 guidelines and using the formal definition of PsB [1,3]. A consort diagram detailing patients and how the samples were used in our study is provided in supplementary material, Figure S1. Ethics guidelines were followed for using archival material for research. This study was approved by the Ethics Committee (CMO) of the RadboudUMC (approval number 2017-3603).

Digital spatial profiling (DSP) experiments and statistical analysis

To characterize intratumoral heterogeneity at the invasive front, eight tissue microarrays (TMAs) consisting of 28 and 36 2-mm cores presenting TB and PsB, respectively, were constructed from formalin-fixed paraffin-embedded (FFPE) resection material of 18 CRC cases. Serial sections (4 μm) of the TMA blocks were cut and mounted onto glass slides. For each TMA, we performed DSP using the NanoString GeoMx DSP platform (NanoString, Seattle, WA, USA) and Cancer Transcriptome Atlas (CTA, NanoString) RNA panel as described previously [4,5]. Antibodies against pan-cytokeratin (PanCK, AE1 + AE3, 1:20, Novus Biologicals, Littleton, CO, USA), CD45 (2B11 + PD7/26, 1:100, Novus Biologicals) and DNA stainSyto13 (121303303, NanoString) were used for immunofluorescent region of interest (ROI) selection. Pathologists (SKO, IDN) preselected ROIs in H&E-stained serial sections of the TMAs and selected the same ROIs in PanCK-positive DSP sections according to ITBCC guidelines and using the formal definition of PsB to ensure that TB or PsB was represented in the ROIs (supplementary material, Figure S2) [1,3]. Tumor areas of interest (AOIs) within the ROI were selected based on PanCK-positive staining, and tumor microenvironment (TME) AOIs were designated PanCK-negative. Only regions contained within the ROIs were utilized in our analyses (supplementary material, Figure S2). Data were preprocessed and normalized using the GeomxTools 3.1.1 package developed by NanoString (https://nanostring.com/resources/analyzing-geomx-ngs-rna-expression-data-with-geomxtools/). Statistical analyses were performed using R version 4.2.0. Differential gene expression across groups was analyzed using linear mixed-effects models [6]. Gene Set Enrichment Analysis (GSEA) was performed using a ranked list of all genes with pathways curated by NanoString. Spatial deconvolution analysis was performed using the SpatialDecon version 1.3 package (https://github.com/Nanostring-Biostats/SpatialDecon/). Differentially expressed genes (DEGs) were defined as $\log_2$ fold-change >0.5 and false discovery rate ≤0.05.

3D immunofluorescence

Thick (80-μm) sections of FFPE resection material containing regions of TB and PsB from two CRC cases were acquired and immunofluorescent staining was performed as described previously [7]. Anti-keratin 18 (DC10, 1:10, Immunologic, Duiven, Gelderland, The Netherlands) and DAPI (D1306, 1:1000, Invitrogen, Waltham, MA, USA) were used for visualizing the tumor and nuclei, respectively. Samples were imaged using confocal microscopy (LSM900, Carl Zeiss, Oberkochen, Germany). FIJI (National Institutes of Health, Bethesda, MD, USA) was used for 3D reconstruction of Z-stacks [8].

Multiplex immunofluorescence (mIF)

Serial sections (4 μm) of TMAs used for DSP were stained using an Opal™ 7 tumor-infiltrating lymphocyte (TIL) panel and myeloid-derived suppressor cell (MDSC) panel (Akoya Biosciences, Marlborough, MA, USA, supplementary material, Table S1), respectively, and analyzed as described previously [9]. The same ROIs as those selected for the DSP analyses (supplementary material, Figure S2) were selected within these serial sections, and only the regions within the ROIs were included in our mIF analysis.

Transmission electron microscopy (TEM)

Samples from three CRC cases where fresh formalin-fixed resection material representing regions of TB and PsB was available were processed and visualized using TEM as described previously [10].

Immunohistochemistry (IHC)

Serial sections (4 μm) of TMAs used for DSP were stained using H&E and for keratin 18 (DC10, 1:160, Immunologic), AE1/AE3 (BS5, 1:800, Sanbio, Uden, North Brabant, The Netherlands), and Ki67 (MIB-1, 1:25, Agilent, Santa Clara, CA, USA) using a DAKO Omnis instrument and the Envision FLEX™ high pH protocol (Agilent), as well as for Fibronectin 1 (FN1, 66042-1-Ig, 1:600, Proteintech, Rosemont, IL, USA), as described previously [11]. The same ROIs selected for the DSP experiments (supplementary material, Figure S2) were selected within these serial sections, and only the regions within the ROIs were included in our IHC analyses. Slides were scanned and Ki67 in all TB and PsB ROIs was quantified using digital pathology (IDS7 version 23.1, Sectra, Linköping, Sweden). Stromal FN1 expression in all TB and PsB ROIs were classified by two independent observers based on intensity as follows: 1, weak; 2, moderate; and 3, strong.

Results

Differences in cellular morphology through 3D visualization and validation using TEM

The PsB region was found to be characterized in three dimensions by cellular debris surrounding a discontinuous epithelial lining (Figure 1B, supplementary material, Video S1). Single cells within the disrupted area were observed as elongated and dissociated with lagging remnants of cell-to-cell adhesions. This may be due to inflammatory cells disrupting the epithelial lining and causing the cells to dissociate. In contrast, within the TB region we did not observe a disrupted epithelial lining (Figure 1A, supplementary material, Video S2). Single cells and cell clusters were observed as intact and displayed a more linearly oriented invasive pattern.

TEM was performed to validate the differences observed in three dimensions and reveal the cellular ultrastructure of both features. A pseudobud (Figure 1D) is observed to be elongated and detached from a larger glandular structure. The cell's membrane is ruptured and surrounded by cellular debris. In contrast, a single tumor
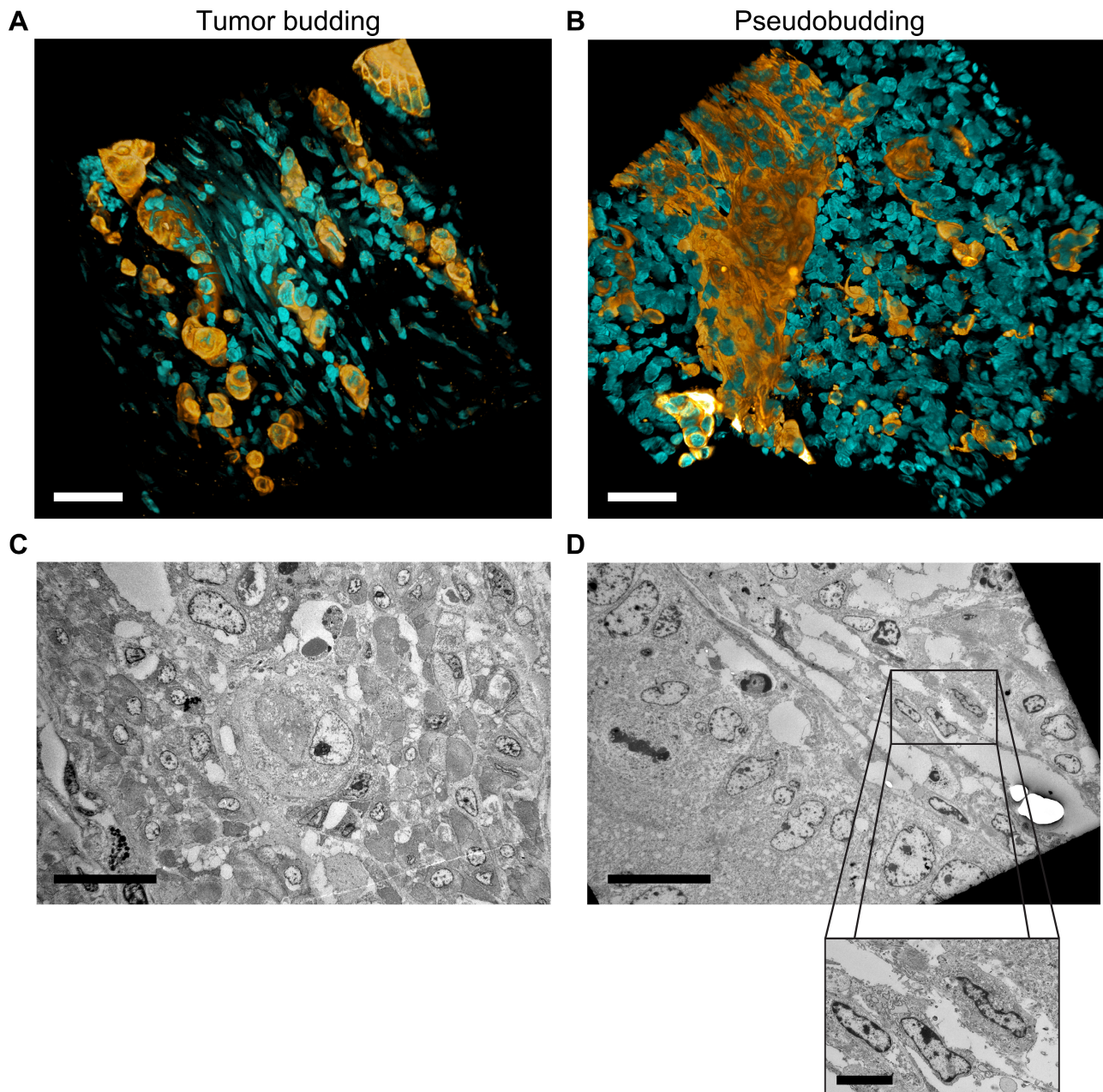
Figure 1. Differences in TB and PsB cellular morphology using 3D and validation through TEM. Three-dimensional (3D) and subcellular visualization of TB and PsB. Thick sections (80 μm) were immunofluorescent stained for cytokeratin 18 (orange) and with DAPI (cyan) to visualize the tumor and nuclei, respectively, and visualized using confocal microscopy. (A) 3D visualization of a TB region. Scale bar, 50 μm. (B) 3D visualization of a PsB region. Scale bar, 50 μm. (C) Subcellular visualization of TB using TEM. Scale bar, 20 μm. (D) Subcellular visualization of PsB using TEM. Scale bar, 20 μm; inset, 5 μm.

bud is revealed to have an intact cell membrane with little to no perturbations in the surrounding tissue structure (Figure 1C).

Phenotypic comparison of TME using mIF

To profile the cellular composition of the TME within the TB and PsB regions, we performed mIF on TMA serial sections using TIL and MDSC panels to quantify immune cell populations (Figure 2A,B). We observed no significant differences in T-cell, B-cell, or natural killer (NK) cell populations (Figure 2C). In contrast, we observed higher densities of granulocytes in PsB regions compared with TB regions (Figure 2D). We also observed significant differences in monocytes, macrophages, and antigen-presenting cell populations (supplementary material, Figure S3).

Distinct transcript profiles and molecular pathways differentiate between TB and PsB regions with validation using IHC

Following preprocessing and normalization, we profiled the expression of over 1,100 unique cancer related gene targets across 321 total samples, of which 166 and 155 represented the tumor (PanCK+) and TME
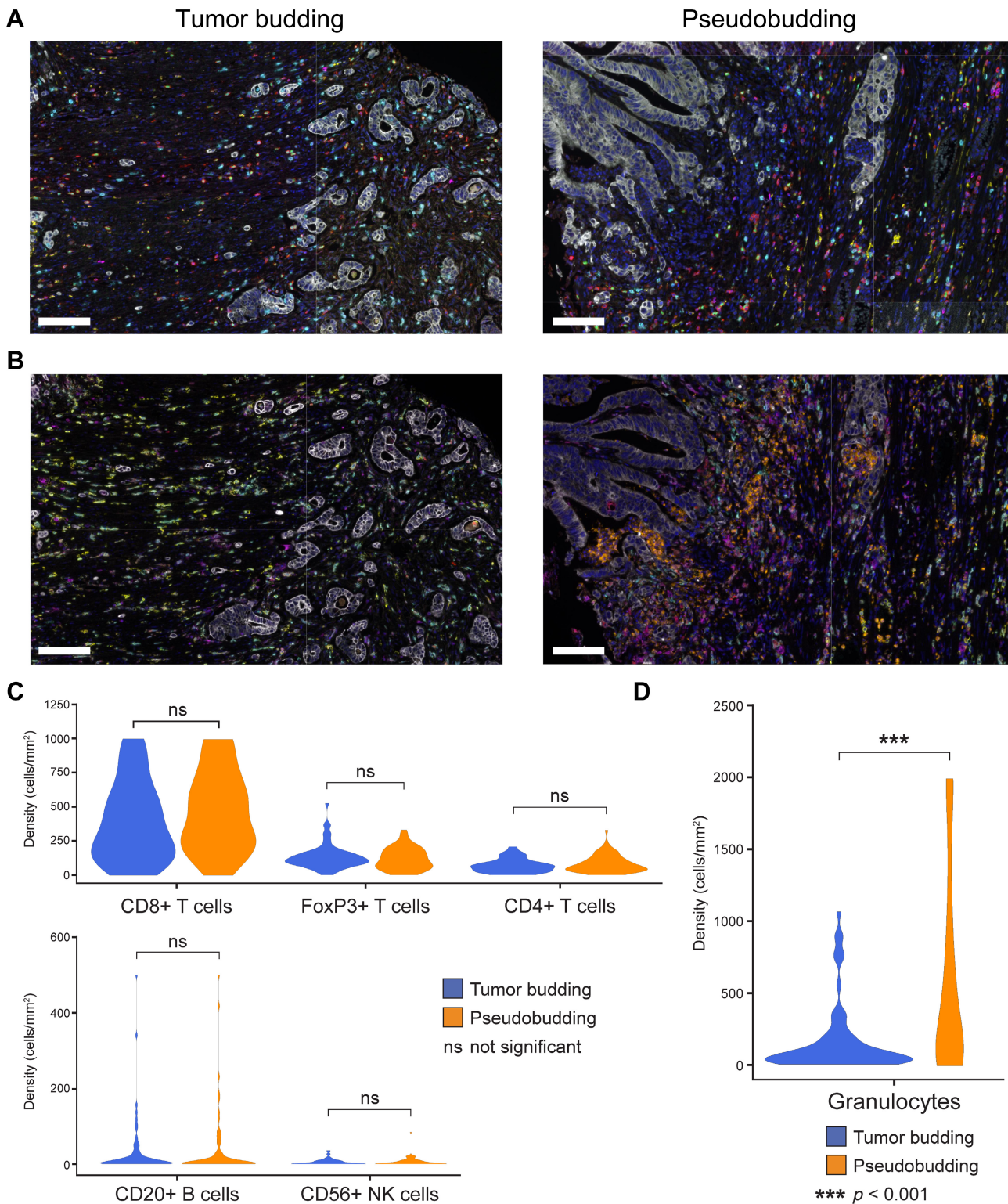
Figure 2. Phenotypic comparison of TME of TB and PsB regions using mIF. Immune microenvironment landscape of TB and PsB regions using mIF. (A) TB (left) and PsB (right) regions stained using TIL panel (AE1/3, tumor, white; CD8, cytotoxic T-cell, cyan; CD20, B-cell, pink; CD56, natural killer (NK) cell, yellow; CD3, helper T-cell, red; FoxP3, T-regulatory cell, red with green nucleus; DAPI, nucleus, blue). White lines and changes in color are due to tiled images. (B) TB (left) and PsB (right) regions stained using MDSC panel (AE1/3, tumor, white; CD163, M2 macrophage, cyan; CD68, Macrophage, red; HLA-DR, Antigen Presenting Cell, purple; CD14, Monocyte, yellow; CD66b, Granulocyte, orange; DAPI, nuclei, blue). White lines and changes in color are due to tiled images. (C) Violin plots showing densities of CD8+ T-cell, FoxP3+ T-cell, CD4+ T-cell, CD20+ B-cell, and CD56+ NK cell populations observed in TB and PsB regions. (D) Violin plot showing densities of granulocytes observed in TB and PsB regions. Scale bars, 100 μm.

(PanCK−), respectively. We found 47 and 24 DEGs to be statistically significant for TB and PsB regions, within the tumor and TME, respectively (Figure 3A and

supplementary material, Table S1). Supervised clustering with the top 100 DEGs separated the TB and PsB regions (supplementary material, Figure S4).

Figure 3   Legend on next page.

GSEA demonstrated that there were differing molecular mechanisms between TB and PsB regions. Within the tumor segment of TB regions, we observed a significant enrichment of pathways involved in cell adhesion and motility, hepatocyte growth factor (HGF) receptor (MET), PDGF, and PI3K-Akt signaling, as well as matrix remodeling, metastasis, and epithelial-mesenchymal-transition (EMT) (Figure 3B). Within the tumor segment of PsB regions, we observed a significant enrichment of pathways involved with the cell cycle, DNA damage repair, and mitochondrial metabolism (Figure 3B). Within the TME segments, we observed a significant upregulation of pathways in TB similar to those of the tumor segments, while in PsB regions we saw a significant enrichment of processes involved with host defense peptides and T-cells (Figure 3B). A full list of GSEA on DSP is provided in supplementary material, Table S1. GSEA for Gene Ontology (GO) revealed processes involved in epithelial migration, extracellular matrix (ECM) organization, and cell cycle progression (supplementary material, Figure S5). *FN1*, involved in migration and metastatic processes, was found to be upregulated in TB regions along with structural components such as collagens IαI, IαII, IIαI, IIIαI, VαI, VαII, VIαIII, and XIαI and cross-linker glycoproteins such as tenascin C (*TNC*) (Figure 3A).

Spatial deconvolution of immune cell populations within the TME showed a significantly higher abundance of fibroblasts and fewer neutrophils within the TB regions (Figure 3C). Ki67, a marker of proliferation, was significantly upregulated in PsB regions (Figure 3A) and validated with IHC staining ($p < 0.001$, *t*-test, Figure 4A). In borderline cases where TB and PsB may be difficult to distinguish, Ki67 staining could be used to help identify TB or PsB (supplementary material, Figure S6). Significantly higher stromal FN1 expression assessed using IHC can be observed in TB regions compared to PsB ($p < 0.001$, *t*-test, Figure 4B). Within the TME of PsB regions, keratin 18 is part of cellular debris, which is not observed in TB (Figure 4C).

Discussion

Through a comprehensive analysis of TB and PsB, our findings clearly established these two features as biologically independent with distinct morphology, microenvironment, and transcriptomic features.

Within TB regions we observed higher RNA expression of extracellular structural components. Coupled with more fibroblasts and FN1, TB regions appeared to have increased deposition of ECM compared to that of PsB. CRCs in which major components of collagen are upregulated have been associated with advanced staging, metastasis, and poor prognosis [12–17]. *In vitro* knockdown of FN1 in CRC cell lines significantly inhibited cellular migration and invasion [18]. TNC may also play a role in driving tumor progression [19]. Based on this evidence, tumor regions exhibiting excessive deposition of ECM may possess significant invasive and metastatic potential [20,21].

PsB regions had more granulocytes within the TME, with a subset of them being neutrophils. Considering the nature of PsB regions where a discontinuous epithelial lining can be observed, granulocytes may play a role in causing glandular disruption. This may also explain the observation of keratin 18-positive cellular debris within the TME because neutrophils can cause damage to surrounding tumor tissue [22].

Within PsB regions, we observed an upregulation of genes associated with cellular division and DNA replication and significantly higher expression of nuclear Ki67 compared to TB. The lack of Ki67 expression is a reported attribute of TB and a hallmark of EMT by increasing cellular survival within the stroma during migration [2]. TB and EMT have also been inextricably linked [2,23]. PsB does not appear to exhibit the same hybrid EMT phenotype observed in TB, which provides further evidence that PsB is disseminated due to glandular disruption.

A study conducted by Oishi *et al* presented cancer gland rupture (CGR) as a potential risk factor for lymph node metastasis (LNM) in early-stage CRC [24]. Moreover, CGR was invariably associated with deep invasion and, to a lesser extent, lymphovascular invasion and TB. No multivariate analysis was performed to establish CGR as an independent risk factor, and associations between CGR and EMT were not investigated. In our study, we performed molecular expression analyses in cancer regions where PsB was present but did not find an association with EMT at either the transcript or protein level. Through a direct comparison with PsB regions, we verify the association of TB regions with EMT and cancer invasion, as have several others [2].

TB regions showed activation of the c-MET/HGF and PDGF pathways, which promote tumor invasion, metastasis, and angiogenesis [25,26]. Potential targeting or inhibition of MET-driven pathways may slow tumor progression [27,28]. PsB regions showed activation of DNA damage repair pathways and host defense peptides, which may be correlated with damage to the tumor

Figure 3. Distinct transcriptional profiles and molecular pathways differentiate between TB and PsB regions. Differential gene expression between TB and PsB regions using DSP. (A) Volcano plot (left) demonstrating DEGs within tumor area of 166 samples presenting TB and PsB, respectively, across 18 CRC cases presenting TB and PsB. *X*-axis shows $-\text{Log}_2$ fold-change and *Y*-axis $-\text{Log}_{10}$ *p* value. Volcano plot (right) demonstrating DEGs within TME of 155 samples presenting TB and PsB, respectively. (B) Bar charts depicting selected significant pathways calculated using gene sets curated by NanoString with genes either upregulated in TB or PsB regions, for tumor (left) and TME (right) segments separately. (C) Spatial deconvolution of immune cell populations within TME of TB and PsB regions, respectively. Statistical comparison used a Wilcoxon test. DC = dendritic cell.
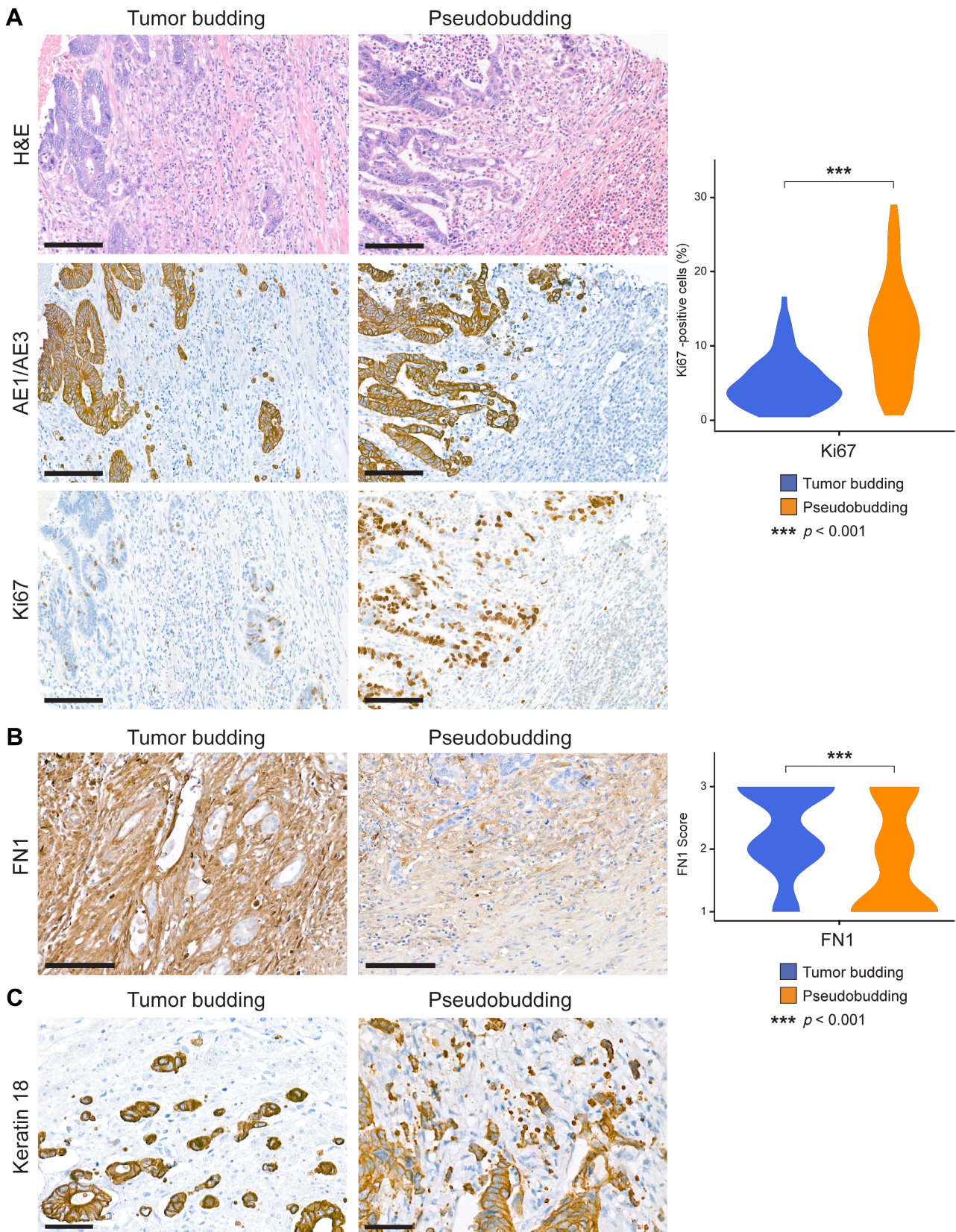
Figure 4. Validation of transcriptomic expression using IHC. IHC validation of transcriptomic expression. Using serial sections of TMAs used for DSP, staining was performed on all TB and PsB regions. (A) Tumor budding (TB) (left) and pseudobudding (PsB) (right) regions stained with H&E (upper), and for pan-cytokeratin (AE1 + AE3) (middle) and Ki67 (lower). Samples depicted are from the same tumor. Violin plot (right) showing percentage of Ki67-positive cells across all TB (blue) and PsB (orange) regions ($p < 0.001$, t-test). Scale bars, 125 μm. (B) TB (left) and PsB (right) regions stained for Fibronectin 1 (FN1). Violin plot (right) showing stromal FN1 expression scored across all TB (blue) and PsB (orange) regions ($p < 0.001$, t-test). Scale bars, 50 μm. (C) TB (left) and PsB (right) regions stained for keratin 18. Keratin 18-positive epithelial debris can be observed in the PsB region. Scale bars, 50 μm.

epithelium caused by immune cells within regions where the host defense is activated. These pathways and mechanisms could be important for the development of future novel biomarkers. This study provides a framework for further research on mechanisms of cancer invasion, tumor heterogeneity, and immune response/activation at the invasive tumor front.

This study has given us insight into tumor heterogeneity and the aspects of tumors that make them particularly invasive and migratory/metastatic in CRC. Previous studies showed that TB regions were characterized by a phenotypic switch from the tumor bulk through the acquisition of migratory characteristics, decreasing cell proliferation, and with TB regions having EMT-positive signatures [29]. Our study characterized TB regions with the same phenotype while highlighting heterogeneity across the invasive front by identifying PsB regions characterized by cell proliferation and lacking EMT-like or migratory signatures.

We did not score PsB in a large series to observe its prognostic effect, nor did we identify specific IHC markers to distinguish TB and PsB. Studies should be conducted to investigate the prognostic value of PsB in a large cohort. Our study did not take into account temporal changes, and, as is inherent in histopathology, looked at a single moment in time which is after the tumor specimen had been excised. At this particular moment, our findings provide evidence to suggest that TB and PsB are features representing differing biological processes. Our findings were made in the context of cancer-specific gene targets and not a whole transcriptome panel. We acknowledge that TB and PsB may be difficult to distinguish when assessed in practice. However, the presence or absence of Ki67 might be a useful tool in cases of doubt (supplementary material, Figure S6).

Several studies confirmed the independent prognostic value of TB in stage II CRCs and for LNM in early-stage CRCs [30–33]. Accurate identification of true tumor buds at the invasive front is important because TB has been found valuable in multiple clinical scenarios: (1) for determining the risk of LNM in patients with early-stage CRC and (2) for identifying patients with high-risk stage II CRC [2]. High-grade TB in early-stage CRC may warrant radical surgery with lymph node dissection. High-grade TB in stage II CRC patients might indicate a potential benefit from adjuvant therapy [2]. We have provided evidence that areas with PsB should be avoided during clinical assessment of TB because their inclusion may lead to an artificially high TB score. With ITBCC guidelines determining TB score based on a range of 0–10 tumor buds, every tumor bud should be accurately identified for effective clinical decision-making.

Acknowledgements

Author contributions statement

TSH, LD, IZ, AL, FS, and IDN designed the experiments, collected data, and carried out the analysis. SKO and IDN selected the cases and ROIs. IDN and NB scored FN1 IHC. TSH and LD prepared the TMA blocks. SV processed the TMA serial sections and mounted them on glass. KV was responsible for mIF staining and scanning. LR and SA carried out the TEM. NR carried out the FN1 IHC staining. TSH, LD, RG, and IJN conducted the DSP experiments. NBJ and CW provided support for the DSP analysis pipeline in R. TSH and IDN designed and coordinated the study. All authors commented on the manuscript and approved its submission for publication.

Data availability statement

The transcriptomics data presented in this study are available in the supplementary material.

References

1. Lugli A, Kirsch R, Ajioka Y, *et al*. Recommendations for reporting tumor budding in colorectal cancer based on the international tumor budding consensus conference (ITBCC) 2016. *Mod Pathol* 2017; **30:** 1299–1311.
2. Lugli A, Zlobec I, Berger MD, *et al*. Tumour budding in solid cancers. *Nat Rev Clin Oncol* 2020; **18:** 101–115.
3. Haddad TS, Lugli A, Aherne S, *et al*. Improving tumor budding reporting in colorectal cancer: a Delphi consensus study. *Virchows Arch* 2021; **479:** 459–469.
4. Zollinger DR, Lingle SE, Sorg K, *et al*. GeoMx™ RNA assay: high multiplex, digital, spatial analysis of RNA in FFPE tissue. *Methods Mol Biol* 2020; **2148:** 331–345.
5. Fisher NC, Byrne RM, Leslie H, *et al*. Biological misinterpretation of transcriptional signatures in tumor samples can unknowingly undermine mechanistic understanding and faithful alignment with preclinical data. *Clin Cancer Res* 2022; **28:** 4056–4069.
6. Bates D, Mächler M, Bolker B, *et al*. Fitting linear mixed-effects models using lme4. *J Stat Softw* 2015; **67:** 1–48.
7. Haddad TS, Friedl P, Farahani N, *et al*. Tutorial: methods for three-dimensional visualization of archival tissue material. *Nat Protoc* 2021; **16:** 4945–4962.
8. Schindelin J, Arganda-Carreras I, Frise E, *et al*. Fiji: an open-source platform for biological-image analysis. *Nat Methods* 2012; **9:** 676–682.

9. Graham Martínez C, Barella Y, Kus Öztürk S, *et al*. The immune microenvironment landscape shows treatment-specific differences in rectal cancer patients. *Front Immunol* 2022; **13**: 1011498.

10. Tizro P, Choi C, Khanlou N. Sample preparation for transmission electron microscopy. *Methods Mol Biol* 2019; **1897**: 417–424.

11. Zhang H, Sun Z, Li Y, *et al*. MicroRNA-200c binding to FN1 suppresses the proliferation, migration and invasion of gastric cancer cells. *Biomed Pharmacother* 2017; **88**: 285–292.

12. Zhang Z, Wang Y, Zhang J, *et al*. COL1A1 promotes metastasis in colorectal cancer by regulating the WNT/PCP pathway. *Mol Med Rep* 2018; **17**: 5037–5042.

13. Wang XQ, Tang ZX, Yu D, *et al*. Epithelial but not stromal expression of collagen alpha-1(III) is a diagnostic and prognostic indicator of colorectal carcinoma. *Oncotarget* 2016; **7**: 8823–8838.

14. Zhang H, Ding C, Li Y, *et al*. Data mining-based study of collagen type III alpha 1 (COL3A1) prognostic value and immune exploration in pan-cancer. *Bioengineered* 2021; **12**: 3634–3646.

15. Niu L, Gao C, Li Y. Identification of potential core genes in colorectal carcinoma and key genes in colorectal cancer liver metastasis using bioinformatics analysis. *Sci Rep* 2021; **11**: 23938.

16. Wang J, Jiang YH, Yang PY, *et al*. Increased collagen type V α2 (COL5A2) in colorectal cancer is associated with poor prognosis and tumor progression. *Onco Targets Ther* 2021; **14**: 2991–3002.

17. Liu W, Li L, Ye H, *et al*. Role of COL6A3 in colorectal cancer. *Oncol Rep* 2018; **39**: 2527–2536.

18. Cai X, Liu C, Zhang TN, *et al*. Down-regulation of FN1 inhibits colorectal carcinogenesis by suppressing proliferation, migration, and invasion. *J Cell Biochem* 2018; **119**: 4717–4728.

19. Yang Z, Zhang C, Feng Y, *et al*. Tenascin-C predicts poor outcomes for patients with colorectal cancer and drives cancer stemness via hedgehog signaling pathway. *Cancer Cell Int* 2020; **20**: 122.

20. Friedl P, Gilmour D. Collective cell migration in morphogenesis, regeneration and cancer. *Nat Rev Mol Cell Biol* 2009; **10**: 445–457.

21. Emon B, Bauer J, Jain Y, *et al*. Biophysics of tumor microenvironment and cancer metastasis – a mini review. *Comput Struct Biotechnol J* 2018; **16**: 279–287.

22. Uribe-Querol E, Rosales C. Neutrophils in cancer: two sides of the same coin. *J Immunol Res* 2015; **2015**: 983698.

23. Grigore AD, Jolly MK, Jia D, *et al*. Tumor budding: the name is EMT. Partial EMT. *J Clin Med* 2016; **5**: 51.

24. Oishi K, Ito T, Sakonishi D, *et al*. Cancer gland rupture as a potential risk factor for lymph node metastasis in early colorectal adenocarcinoma with deep submucosal invasion. *Histopathology* 2020; **76**: 603–612.

25. Chen J, Yuan W, Wu L, *et al*. PDGF-D promotes cell growth, aggressiveness, angiogenesis and EMT transformation of colorectal cancer by activation of Notch1/Twist1 pathway. *Oncotarget* 2017; **8**: 9961–9973.

26. Fu J, Su X, Li Z, *et al*. HGF/c-MET pathway in cancer: from molecular characterization to clinical evidence. *Oncogene* 2021; **40**: 4625–4651.

27. Trusolino L, Bertotti A, Comoglio PM. MET signalling: principles and functions in development, organ regeneration and cancer. *Nat Rev Mol Cell Biol* 2010; **11**: 834–848.

28. Xie YH, Chen YX, Fang JY. Comprehensive review of targeted therapy for colorectal cancer. *Signal Transduct Target Ther* 2020; **5**: 22.

29. De Smedt L, Palmans S, Andel D, *et al*. Expression profiling of budding cells in colorectal cancer reveals an EMT-like phenotype and molecular subtype switching. *Br J Cancer* 2017; **116**: 58–65.

30. Ueno H, Ishiguro M, Nakatani E, *et al*. Prospective multicenter study on the prognostic and predictive impact of tumor budding in stage II colon cancer: results from the SACURA trial. *J Clin Oncol* 2019; **37**: 1886–1894.

31. Lee SJ, Kim A, Kim YK, *et al*. The significance of tumor budding in T1 colorectal carcinoma: the most reliable predictor of lymph node metastasis especially in endoscopically resected T1 colorectal carcinoma. *Hum Pathol* 2018; **78**: 8–17.

32. Romiti A, Roberto M, Marchetti P, *et al*. Study of histopathologic parameters to define the prognosis of stage II colon cancer. *Int J Colorectal Dis* 2019; **34**: 905–913.

33. Nearchou IP, Kajiwara Y, Mochizuki S, *et al*. Novel internationally verified method reports desmoplastic reaction as the most significant prognostic feature for disease-specific survival in stage II colorectal cancer. *Am J Surg Pathol* 2019; **43**: 1239–1248.

SUPPLEMENTARY MATERIAL ONLINE

Figure S1. Consort diagram of patients and sample use

Figure S2. NanoString GeoMx regions of interest

Figure S3. MDSC panel multiplex immunofluorescence (mIF) data

Figure S4. Top 100 DEGs – tumor

Figure S5. Gene Set Enrichment Analysis (GSEA) for Gene Ontology (GO) – tumor

Figure S6. Borderline cases and use of Ki67 staining

Table S1. Clinical demographic data of patients, tumor-infiltrating lymphocyte (TIL) panel, myeloid-derived suppressor cell (MDSC) panel, full NanoString data analysis (DEGs, tumor, and TME), full GSEA results (tumor and TME).

Video S1. Pseudobudding in 3D

Video S2. Tumor budding in 3D